CHALMERS
UNIVERSITY OF TECHNOLOGY

A Two-Stage MIQP-Based Optimization Approach for Coordinating Automated Electric Vehicles in Confined Sites

Citation for the original published paper (version of record):
Kojchev, S., Hult, R., Fredriksson, J. et al (2024). A Two-Stage MIQP-Based Optimization Approach for Coordinating Automated Electric Vehicles in
Confined Sites. IEEE Transactions on Intelligent Transportation Systems, 25(2): 2061-2075.
http://dx.doi.org/10.1109/TITS.2023.3320168

A Two-Stage MIQP-based Optimization Approach for Coordinating Automated Electric Vehicles in Confined Sites

Stefan Kojchev, Robert Hult, Jonas Fredriksson and Maximilian Kneissl

***Abstract*—In this paper, we present a high-level optimization-based control strategy for the coordination of electric automated vehicles (AVs) in confined sites. A centralized controller optimizes the state and input trajectories of all vehicles in the site such that collisions are avoided in cross-intersections, narrow roads, merge crossings, and charging stations, while also considering the charging process. Specifically, the controller consists of two optimization-based components. The first component is tasked with solving the combinatorial part of the problem, which corresponds to the order in which the vehicles pass the crossings, by solving a Mixed Integer Quadratic Problem (MIQP). The found combinatorial solution is then utilized for calculating the optimal state and input trajectories that are obtained by solving a Nonlinear Program (NLP). The control algorithm is compared with respect to alternative optimization-based approaches in simulation scenarios. For the presented scenario, our method achieves improved energy efficiency by up to 7.6% while slightly improving the average mission end time, and furthermore, it is capable of avoiding deadlocks.**

***Index Terms*—Autonomous vehicles, electric vehicles, motion control, optimal scheduling, vehicle safety.**

I. Introduction

CONFINED sites, such as ports, logistic centers, mines, etc., describe the use case when in an enclosed environment a known amount of vehicles and/or machines are required to accomplish a site-specific goal, for example, extract the desired amount of ore per day. To reduce CO2 emissions, the site operators request to replace internal combustion vehicles with electric vehicles. However, to retain productivity, more electric vehicles would be required, due to limitations such as range and towing capacity. To avoid increased personnel costs, it is necessary to automate the operation of the vehicles with the goal of improving site productivity.

Deploying automated vehicles (AVs) in confined sites is a reachable near-future goal, as mainly by construction, confined sites avoid some of the barriers that exist in deploying AVs on public roads [1]. Specifically, confined sites can be designed such that all vehicles operating in the site are known and there are no unsupervised actors, which dramatically reduces safety concerns. Moreover, by coordinating the vehicles on the site, the same productivity targets (e.g., the amount of transported material per day) can potentially be reached with fewer vehicles. For confined sites, it can be assumed that wireless coverage is good and that there exists a central computational resource, capable of distributing information to the vehicles. Figure 1 shows an example of a confined quarry site with multiple trucks and wheel loaders collaborating using the communication and computing center in the top left part of the figure. The communication and computing center is in charge of distributing the necessary information to the vehicles regarding tasks they need to perform and plan their motion. The general problem on such sites is to utilize the available resources, e.g., machines, vehicles, and roads efficiently in order to meet productivity requirements [2]. This includes decisions that couples task allocation (which vehicle does what), task scheduling (which task should be done first), routing (which vehicle uses what road), and motion planning (how should the vehicles move). The problem easily results in an intractable large-scale computational problem. It is thus desirable to decompose the site problem into multiple tractable sub-problems. A proposed decomposition of the problem in form of a system architecture is given in Figure 2. The "Mission planner" component assigns each available vehicle a transport mission. A transport mission is a vague

This work is partially funded by Sweden's innovation agency Vinnova, project number: 2018-02708.

Fig. 1. Example of a confined site with multiple workstations and operating vehicles.

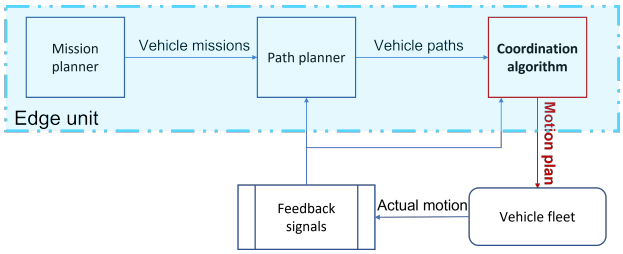

Fig. 2. Architecture of the fleet motion planning system.

description of what should be achieved and which control points (loading/unloading zones, charging zones, etc.) should be visited, for example, Vehicle 1 should load a specific amount from mining point A, Vehicle 2 should charge at charging station C, etc. The "Path planner" then obtains the paths (routes) of the vehicles such that the control points are respected and form the road network. Using the road network, the "Coordination algorithm" is tasked to compute the state and input trajectories for all vehicles such that joint utilization of the control points and other inter-vehicle conflicts are avoided. This paper focuses on how the coordination task is achieved. In general, the coordination problem is difficult to solve and is formally shown to be NP-hard in [4]. The control points where the vehicles need to share a resource and the parts of the road network where an inter-vehicle conflict can occur are also known as MUTually EXclusive (MUTEX) zones. Examples of MUTEX zones are charging stations, loading/unloading zones, intersections, narrow roads, merge-splits, etc. Each MUTEX zone implies that there should be an order in which the vehicles cross the zone. This combinatorial decision is the predominant component in the complexity of the coordination problem. Commonly proposed approaches leverage optimal control methods, often relying on simplifying assumptions and heuristics, to compute the coordinated vehicle trajectories [5]- [9]. The motion trajectories of all vehicles are assembled into a motion plan that is communicated to the "Vehicle fleet", which follows the plan and sends feedback on the execution of the plan.

A. Related Work

For public roads, the safe and efficient coordination of multiple AVs in MUTEX zones, in most cases focusing on intersections, has received substantial attention, see [3] for a comprehensive survey. Common approaches leverage Model Predictive Control (MPC) [10], [11], [12], consensus-based methods [13], [14], direct optimal control [15], [16], [17], and trajectory optimization methods [18], [19], [20], for solving the problem.

Coordination of AVs in confined sites has some distinct differences compared to the intersection scenarios. Specifically, as the road network is known it is possible to plan the motion of the vehicles from the start of a transport mission to its end. Planning the motion over long horizons is particularly beneficial in terms of energy efficiency [21]. Furthermore, confined areas have additional MUTEX zones besides intersections as mentioned earlier. A consequence of long-horizon planning is that a vehicle can experience multiple combinations of the MUTEX zones along its route. The authors in [22] and [23] propose approaches on multiple intersection coordination, however, consider a "cut-out" around the intersections with vehicles arriving at speed in comparison to the desired full route motion planning that considers all MUTEX zones at the planning stage.

Another studied problem is coordination in valet parking applications [24]. This application has a lot of similarities with coordinating vehicles in confined sites, namely both applications consider a closed-off area where the vehicles can experience multiple MUTEX zones of different types, [25]. The contribution of this article presents an alternative optimization-based heuristic from the approaches considering the valet parking application [25], [26]. Furthermore, in valet parking, vehicles move at low speeds which helps in providing safety guarantees, while in confined sites, it is desirable for vehicles to move at higher speeds to increase productivity. In addition, the valet parking applications have laxer energy efficiency and productivity goals.

Dynamic fleet planning method for autonomous mining is proposed in [27]. The method focuses on solving conflicts efficiently while attempting to minimize delays and waiting times by using a modified genetic algorithm. The approach, however, neglects vehicle dynamics and requires locations and time for the vehicles to stand still, which might lead to suboptimal behavior.

Solving the coordination problem has also been addressed for industrial robots, see e.g., [28] and [29]. The robotics research field has explored different solving algorithms and ways of approximating the problem, see [30]. In general, for the vehicle problem, the dynamics and road topography play a significant role in the optimization problem, which is often, justifiably, neglected or simplified in the case of industrial robots.

B. Contributions

In our previous work [31] and [32], we proposed optimization-based heuristics to coordinate vehicles in confined sites, ensuring conflict avoidance in all MUTEX zones.

This paper introduces a control strategy that extends the optimal control formulation from [32] to address the inclusion of charging zone MUTEX constraints. To capture the intricacies of the charging process, we incorporate models that represent electric vehicles' powertrain dynamics. In terms of analysis, we evaluate the proposed approach in comparison to alternative optimization-based heuristics.

One significant aspect of our work is the inclusion of charging MUTEX zones, which has received limited attention in the context of confined site vehicle coordination. This task is non-trivial and arises from industry feedback highlighting the necessity to accommodate electric vehicles. While the heuristic idea and general approach remain consistent with [32], we extend the framework to effectively handle the coordination of vehicles within charging zones and during the charging process. By incorporating charging MUTEX zones, our approach becomes more comprehensive and applicable.

Although focusing on electric vehicles, the coordination strategy presented in this paper is not restricted by a specific choice of motion models, constraints, or objective functions. Furthermore, while the approach is adapted to the confined site requirements (i.e., solving the problem centrally for the entire path of the vehicles, including multiple MUTEX zones), the heuristic could be easily adapted to other use cases, for example, coordination of fully automated vehicles at intersections.

C. Outline

The remainder of the paper is organized as follows: In Section II we define the system model and MUTEX constraints and state the confined site coordination problem. Section III provides the specific electric vehicle model that is used in this paper. In Section IV, we present the Optimal Control Problem (OCP) definition, accompanied by a decomposition strategy employed to enhance computational tractability. In Section V and Section VI the approach is evaluated with respect to different baselines through simulation examples. Finally, the paper is concluded in Section VII with a discussion of the contributions and possible extensions.

II. Problem Formulation

We consider a road network of N_a fully automated vehicles traversing in a confined area, meaning that non-controlled traffic participants such as pedestrians, manually operated vehicles, bicycles, etc., are absent.

In order to ease the comprehension of the modeling, the reader is referred to Table IV in the Appendix, which offers a detailed summary of all the notations introduced throughout the paper.

A. System Model

Assume that the vehicles move along fixed and known paths and that no vehicle reverses and that overtaking is prohibited. The vehicle motion along the path can, without restriction from the above-mentioned assumption, be described as

$$\dot{p}_i(t) = v_i(t) \tag{1}$$
$$\dot{x}_i(t) = f_i(p_i(t), x_i(t), u_i(t)) \tag{2}$$
$$0 \leq h_i(p_i(t), x_i(t), u_i(t)). \tag{3}$$

where $p_i(t) \in \mathbb{R}$ is the vehicle's position, $x_i(t) \in \mathbb{R}^n$ is the vehicle state, $u_i(t) \in \mathbb{R}^m$ is the control input, with $i \in \{1, \ldots, N_a\}$. The state is subdivided as $x_i(t) = (v_i(t), z_i(t))$, with the speed along the path $v_i(t) \in \mathbb{R}$ and $z_i(t) \in \mathbb{R}^{n-1}$ collecting possible other states. The functions f_i and h_i, both assumed smooth, describe the dynamics and constraints that capture, e.g., actuator and state limitations.

Remark 1: Note that the remaining possible states $z_i(t)$ directly depend on the choice of a vehicle model. For example, if the vehicle is modeled as a triple integrator $\dddot{x}(t) = u(t)$, the remaining vehicle states are $z_i(t) = a_i(t)$, with $a_i(t)$ being the acceleration. The state variables are thus $p_i(t),\ x_i(t) = (v_i(t), a_i(t))$.

B. System Model in the Spatial Domain

As stated in [32], for confined site optimization, it is beneficial to optimize the trajectories of the vehicles over their full paths. However, the time it takes a vehicle to traverse a path is dependent on the solution, and not known *a-priori*. Consequently, it is inappropriate to plan the vehicle's motion with time as the independent variable. The motion model (1) can be reformulated in the spatial domain using that $\frac{\mathrm{d}p_i}{\mathrm{d}t} = v_i(t)$ and $\mathrm{d}t = \mathrm{d}p_i / v_i(t)$:

$$\frac{\mathrm{d}t_i}{\mathrm{d}p_i} = \frac{1}{v_i(p_i)} \tag{4}$$
$$\frac{\mathrm{d}x_i}{\mathrm{d}p_i} = \frac{1}{v_i(p_i)} f_i(p_i, x_i(p_i), u_i(p_i)) \tag{5}$$
$$0 \leq h(p_i, x_i, u_i). \tag{6}$$

This leads to that position is now the independent variable and that travel time t_i is a state variable.

Remark 2: Note that equation (4) imposes that the velocity must be strictly positive.

C. MUTEX Zones Modeling

The safety constraints ensure a collision-free crossing of the MUTEX zones, that the vehicles encounter. In this paper, we consider four types of conflict zones, intersection-like, narrow road, merge-split, and charging stations, all zones depicted in Figure 3. A MUTEX zone is defined by the entry and exit position $[p_i^{in}, p_i^{out}]$ on the path of each vehicle. From the known positions, the time of entry and exit of Vehicle i is $t_i^{in} = t_i(p_i^{in})$ and $t_i^{out} = t_i(p_i^{out})$, respectively.

1) Narrow road and intersection-like zones: In the narrow road MUTEX zones, meeting oncoming vehicles is not possible. From a safety perspective, this translates to "reserving" the zone for one or more vehicles coming from the same direction. The vehicles coming from the opposite direction are not allowed to occupy the zone until it is vacated. The intersection-like MUTEX zone is similar to the narrow road in terms of its safety requirement, i.e., vehicle j is not allowed to enter the MUTEX zone before vehicle $i \neq j$ exits the MUTEX zone, or vice-versa. Let $\mathcal{I} = \{I_1, I_2, ..., I_{r_0}\}$ denote the set of all intersections and narrow roads in the confined area, with r_0 being the total number of intersections and narrow roads, and $\mathcal{Q}_r = \{q_{r,1}, q_{r,2}, ..., q_{r,l}\}$ denote the set of vehicles that cross an intersection or narrow road I_r. The order in which the vehicles cross the zones I_r is denoted $\mathcal{O}_r^{\mathcal{I}} = \left(s_{r,1}, s_{r,2}, ..., s_{r,|\mathcal{Q}_r|}\right)$, where $s_{r,1}, s_{r,2}, ...$ are vehicle indices and $\mathcal{O}^{\mathcal{I}} = \left\{\mathcal{O}_1^{\mathcal{I}}, \ldots, \mathcal{O}_r^{\mathcal{I}}\right\}$ is the collection of all crossing order sets for these zones. A sufficient condition for collision avoidance for the r-th intersection or narrow road MUTEX zone can be formulated as

$$t_{s_{r,i}}(p^{\text{out}}_{s_{r,i}}) \leq t_{s_{r,i+1}}(p^{\text{in}}_{s_{r,i+1}}),\ i \in \mathbb{I}_{[1,|\mathcal{Q}_r|-1]}, \tag{7}$$

where t is determined from (4).

2) Merge-split zones: In the merge-split case, two vehicles coming from different roads, but moving in the same direction of travel, join together on a common patch of road. After some distance, the roads separate. For this type of MUTEX zone, let $\mathcal{MS} = \{MS_1, MS_2, ..., MS_{w_0}\}$ denote a set of all merge-split zones, with w_0 being the total number of merge-split zones in the site and $\mathcal{Z}_w = \{z_{w,1}, z_{w,2}, ..., z_{w,h}\}$ denote the set of vehicles that cross the merge-split zone MS_w. For efficiency, it is desirable to have several vehicles in the zone at the same time, instead of blocking the whole zone. This requires imposing rear-end collision constraints once the vehicles have entered the merge-split zone. In this case, the order

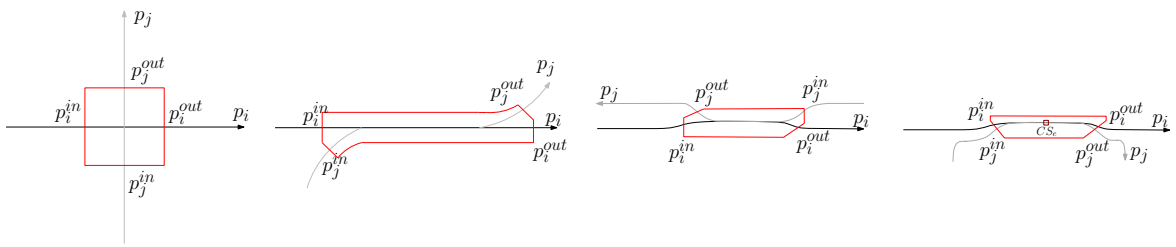

a) Intersection-like b) Merge-split c) Narrow road d) Charging station

Fig. 3. Types of conflict zones.

in which the vehicles enter the zone is denoted as $\mathcal{O}_w^{\mathcal{MS}} = \left(s_{w,1}, s_{w,2}, ..., s_{w,|\mathcal{Z}_w|}\right)$, and let $\mathcal{O}^{\mathcal{MS}} = \left\{\mathcal{O}_1^{\mathcal{MS}}, \ldots, \mathcal{O}_w^{\mathcal{MS}}\right\}$ be the collection of all crossing order sets for the merge-split zones. The collision avoidance requirement for the w-th merge-split zone is described with the following constraints:

$$t_{s_{w,i}}(p^{\text{in}}_{s_{w,i}}) + \Delta t \leq t_{s_{w,i+1}}(p^{\text{in}}_{s_{w,i+1}} - c) \tag{8a}$$

$$t_{s_{w,i},k_i} + \Delta t \leq t_{s_{w,i+1}}(p_{s_{w,i},k_i} - p^{\text{in}}_{s_{w,i}} + p^{\text{in}}_{s_{w,i+1}} - c),$$

$$k^{\text{in}}_{s_{w,i}} \leq k_i \leq k^{\text{out}}_{s_{w,i}} \tag{8b}$$

$$t_{s_{w,i}}(p^{\text{out}}_{s_{w,i}}) + \Delta t \leq t_{s_{w,i+1}}(p^{\text{out}}_{s_{w,i+1}} - c), \tag{8c}$$

$$i \in \mathbb{I}_{[1,|\mathcal{Z}_w|-1]},$$

where k_i is an index of the position vector $p_{s_{w,i}}$.

Constraint (8) ensures that while in the MUTEX zone, the vehicles must be separated by at least a time-period Δt and a distance c, depending on if vehicle j is in front of vehicle i or vice versa. This is equivalent to the standard offset and time-headway formulation often used in automotive adaptive cruise controllers [33].

Remark 3: Road merges and road splits are a subset of the merge-split zones. For the road merges case, we can impose the same constraints as in (8) without the (8c) constraint, while the road splits we impose the constraints in (8) without the (8a) constraint.

3) Charging Stations: We define charging stations as a zone the vehicles are assigned to visit by the mission planner component. The station consists of a road patch that leads to the charger and a road patch after the charger until a merge point with the remainder of the road. When a vehicle visits a charging station, it is required to make a full stop at the charger and after some charging time, $t_{\text{charge},i}$ the vehicle leaves the station with an increased state of charge. The advantage of utilizing a spatial model is that time is a state variable. To account for the charging time, we can modify the time state constraint by adding the duration of the charging process. Essentially, the time state after the charger location is:

$$t_{i,\text{CS}+1} = t_{i,CS+1} + t_{\text{charge},i}, \tag{9}$$

where CS is the position of the charger.Note that the charging time is communicated and decided by the mission planner component. The increase in the state of charge depends directly on the charging time and the capacity of the charging stations.

In the case when two, or more, vehicles are assigned to the charging station, the algorithm needs to enforce rear-end constraints for collision avoidance. We formalize the constraints by first defining a set of all charging station zones as $\mathcal{CS} = \{CS_1, CS_2, ..., CS_{e_0}\}$, with e_0 being the total number of charging station zones in the site. Furthermore, let $\mathcal{G}_e = \{g_{e,1}, g_{e,2}, \ldots, g_{e,y}\}$ denote the set of vehicles that utilize the charging station CS_e. The order in which the vehicles utilize the charging station is denoted as $\mathcal{O}_e^{\mathcal{CS}} = \left(s_{e,1}, s_{e,2}, ..., s_{e,|\mathcal{G}_e|}\right)$ and $\mathcal{O}^{\mathcal{CS}} = \left\{\mathcal{O}_1^{\mathcal{CS}}, \ldots, \mathcal{O}_w^{\mathcal{CS}}\right\}$ is the collection of all crossing order sets for the charging zones. The collision avoidance constraints for the e-th charging station zone are thus stated as

$$t_{s_{e,i}}(p^{\text{in}}_{s_{e,i}}) + \Delta t \leq t_{s_{e,i+1}}(p^{\text{in}}_{s_{e,i+1}} - c) \tag{10a}$$

$$t_{s_{e,i},k_i} + \Delta t \leq t_{s_{e,i+1}}(p_{s_{e,i},k_i} - p^{\text{in}}_{s_{e,i}} + p^{\text{in}}_{s_{e,i+1}} - c),$$

$$k^{\text{in}}_{s_{e,i}} \leq k_i < k^{\text{charge}}_{s_{e,i}} \tag{10b}$$

$$v_{s_{e,i},k_i} = \underline{v}_{s_{e,i}}, \quad k_i = k^{\text{charge}}_{s_{e,i}} \tag{10c}$$

$$t_{s_{e,i},k_i} = t_{s_{e,i},k_i} + t_{\text{charge},i}, \quad k_i = k^{\text{charge}}_{s_{e,i}} + 1 \tag{10d}$$

$$t_{s_{e,i},k_i} + \Delta t \leq t_{s_{e,i+1}}(p_{s_{e,i},k_i} - p^{\text{in}}_{s_{e,i}} + p^{\text{in}}_{s_{e,i+1}} - c),$$

$$k^{\text{charge}}_{s_{e,i}} + 1 \leq k_i \leq k^{\text{out}}_{s_{e,i}} \tag{10e}$$

$$t_{s_{w,i}}(p^{\text{out}}_{s_{e,i}}) + \Delta t \leq t_{s_{e,i+1}}(p^{\text{out}}_{s_{e,i+1}} - c), \tag{10f}$$

$$i \in \mathbb{I}_{[1,|\mathcal{G}_e|-1]},$$

where $k^{\text{charge}}_{s_{e,i}}$ is the index where the vehicle position is at the charger location.

Remark 4: The vehicles are required to make a full stop at the charger, however, as noted by Remark 2, this is restricted when using a model in the spatial domain. This restriction imposes that the "Vehicle fleet" model and logic must take the vehicles to a full stop and form a queue where the preceding vehicles wait behind the charging vehicle at a sufficient distance.

D. A practical reformulation of the collision constraints

A common way to handle constraints such as (7), (8) and (10) is to introduce auxiliary binary variables and use the "big-M" technique [37]. For example, an equivalent representation to the constraint (7), is

$$t_{s_{r,i}}(p^{out}_{s_{r,i}}) - t_{s_{r,i+1}}(p^{in}_{s_{r,i+1}}) \leq b_{s_r,i,i+1}M, \tag{11a}$$

$$t_{s_{r,i+1}}(p^{out}_{s_{r,i+1}}) - t_{s_{r,i}}(p^{in}_{s_{r,i}}) \leq (1 - b_{s_r,i,i+1})M. \tag{11b}$$

where $b_{s_r,i,i+1} \in \{0,1\}$, $i \in \mathbb{I}_{[1,|\mathcal{Q}_r|-1]}$ and M a sufficiently large positive number. In the case where $b_{s_r,i,i+1} = 0$, the vehicle $i+1$ is constrained to cross the MUTEX zone after

the vehicle i, with the opposite being true if $b_{s_r,i,i+1} = 1$. We collect all integer variables for all MUTEX zones in $b \in \mathbb{Z}_2^{r_o+w_0+e_0}$.

E. Optimal coordination problem

The problem of finding the optimal vehicle trajectories that avoid collisions in the general case can be formulated as:

***Problem** 1:* (Optimal coordination problem) Obtain the optimal state and control trajectories $\mathcal{X}^* = \{x_1^*, ..., x_{N_a}^*\}, \mathcal{U}^* = \{u_1^*, ..., u_{N_a}^*\}$, given the initial state $\mathcal{X}_0 = \{x_{1,0}, ..., x_{N_a,0}\}$, by solving the optimization problem

$$\min_{x_i,u_i,\mathcal{O}^{\mathcal{I}},\mathcal{O}^{\mathcal{MS}},\mathcal{O}^{\mathcal{CS}}} \quad \sum_{i=1}^{N_a} J_i(x_i,u_i) \tag{12a}$$

$$\text{s.t.} \quad \text{initial states} \;\; x_{i,0} = \hat{x}_{i,0}, \forall i \tag{12b}$$

$$\text{system dynamics} \;\; (4),(5) \; \forall i, \tag{12c}$$

$$\text{state and input constraints} \;\; (6), \; \forall i, \tag{12d}$$

$$\text{safety constraints} \;\; (7),(8),(10) \; \forall i, \tag{12e}$$

Note in particular that this involves finding the crossing orders $\mathcal{O}^{\mathcal{I}}$, $\mathcal{O}^{\mathcal{MS}}$, $\mathcal{O}^{\mathcal{CS}}$ which makes the problem combinatorial and expensive to solve.

III. Electric Vehicle Model

In this section, the longitudinal dynamics that describe the motion of the electric vehicles are derived.

A. Longitudinal Dynamics

The longitudinal dynamics of an electric vehicle in the spatial domain can be described using Newton's second law of motion

$$\frac{\mathrm{d}t_i}{\mathrm{d}p_i} = \frac{1}{v_i(p_i)} \tag{13a}$$

$$\frac{\mathrm{d}v_i}{\mathrm{d}p_i} = \frac{1}{v_i(p_i)} \frac{1}{m_i} \left(F_{M,i}(p_i) - F_{d,i}(p_i,v_i) - F_{rg,i}(p_i)\right), \tag{13b}$$

where p_i, v_i and m_i are Vehicle i's position, velocity and mass, respectively. The forces are the electric motor force $F_{M,i}$, which is used for both propelling and braking the vehicle, the aerodynamic drag $F_{d,i}$, and the rolling resistance and gravitational load $F_{rg,i}$. The aerodynamic drag, rolling resistance, and gravitational load can be described as

$$F_{d,i}(p_i,v_i) = \frac{1}{2}\rho A_i c_{a,i} v_i(p_i)^2 \tag{14a}$$

$$F_{rg,i}(p_i,t) = m_i g(sin(\theta(p_i)) + c_{r,i} cos(\theta(p_i)), \tag{14b}$$

where ρ is the air density, A_i is the frontal area of the vehicle, $c_{a,i}$ is the aerodynamic drag coefficient, $c_{r,i}$ is the rolling resistance coefficient and θ is the road gradient.

As mentioned in Remark 2, a price to pay for the spatial domain representation is that the velocity cannot be zero, as implied by (13a). This limitation of the model enforces a minimum velocity bound $\underline{v}$. Practically, this constraint is not restricting, particularly as the scheme developed in this paper acts as a high-level controller. In addition, the velocity is limited by the confined site speed limits or the vehicle's physical speed limits. The velocity is thus constrained by

$$\underline{v}_i \leq v_i(p_i) \leq \overline{v}_i. \tag{15}$$

Furthermore, we bound the longitudinal acceleration of the vehicle

$$\underline{a}_{i,\text{lon}} \leq a_i(p_i) \leq \overline{a}_{i,\text{lon}}, \tag{16}$$

and also impose constraints resulting from the curvature of the road. When the vehicles operate on curved roads they experience lateral forces, and as the one-dimensional model that is used in this paper does not account for lateral motion, the following constraint is enforced

$$\left(\frac{a_i(p_i)}{\overline{a}_{i,\text{lon}}}\right)^2 + \left(\frac{\kappa_i(p_i) v_i(p_i)^2}{\overline{a}_{i,lat}}\right)^2 \leq 1, \tag{17}$$

where $\overline{a}_{i,lat}$ is the lateral acceleration limit and $\kappa_i(p_{i,k})$ is the road curvature, that is assumed to be available at every point along the path.

B. Electric Powertrain

The electric machine is coupled to a gearbox and battery to form the powertrain of the electric vehicle.

1) Battery: In comparison to some other approaches that use a similar modeling technique such as [34], we the battery as an ideal voltage source with an internal resistance. We thus define battery power as the difference between the product of velocity and motor force and the internal battery losses due to the resistance as

$$P_{b,i}(v_i, F_{M,i}) = F_{M,i}(p_i) v_i(p_i) - P_{\text{loss}} \tag{18}$$

$$\underline{P}_{b,i} \leq P_{b,i} \leq \overline{P}_{b,i}, \tag{19}$$

with $\underline{P}_{b,i}, \overline{P}_{b,i}$ representing the power limits, and

$$P_{\text{loss}} = \frac{R_{\text{int,i}} N_{\text{cells,i}}}{K_{t,i}^2} T_{M,i}^2 \tag{20}$$

where $R_{\text{int,i}}$ is the internal resistance of the battery, $N_{\text{cells,i}}$ is the number of cells of the battery, $K_{t,i}$ represents the electric machine's torque constant and $T_{M,i}$ is the motor torque defined in the following.

Furthermore, we define the state of charge (SOC) of the battery as a state governed by the following equation

$$\frac{\mathrm{dSOC}_i}{\mathrm{d}p_i} = \frac{-P_{b,i}(v_i(p_i), F_{M,i}(p_i))}{E_{b,\max,i}}, \tag{21}$$

where $E_{b,\max,i}$ is the maximum energy capacity of the battery. The state of charge is constrained by a lower and upper bound, i.e.,

$$\underline{\text{SOC}}_i \leq \text{SOC}_i \leq \overline{\text{SOC}}_i. \tag{22}$$

2) Gearbox: The powertrain of electric trucks consists of several electric motors coupled to a gearbox with a high number of gears. We model the gearbox as a Continuous Variable Transmission (CVT) [35]. This modeling choice leads to a new input variable $M_{\text{CVT},i}(p_i)$ representing the gear ratio, which is bounded by

$$1 \leq M_{\text{CVT},i}(p_i) \leq M_{f,i}. \tag{23}$$

where $M_{f,i}$ is the transmission's final gear ratio. Consequently, the powertrain torque is limited to

$$\underline{T}_{M,i} \leq \frac{r_{w,i} F_{M,i}(p_i)}{M_{\text{CVT},i}(p_i)} \leq \overline{T}_{M,i}, \tag{24}$$

where $r_{w,i}$ is the wheel radius.

Remark 5: Modeling gearboxes and the shifting strategy is a non-trivial problem of its own [36]. The modeling simplification we make in this paper is sufficient for the high-level control problem we want to solve.

C. Complete Vehicle Model

With the defined electric powertrain, we can assemble the complete vehicle model that is used in this article as

$$\frac{\mathrm{d}t_i}{\mathrm{d}p_i} = \frac{1}{v_i(p_i)} \tag{25a}$$

$$\frac{\mathrm{d}v_i}{\mathrm{d}p_i} = \frac{1}{v_i(p_i)} \frac{1}{m_i} \Bigg(F_{M,i}(p_i) - \frac{1}{2} \rho A_i c_{a,i} v_i(p_i)^2 - m_i g \Big(sin\big(\theta(p_i)\big) + c_{r,i} cos\big(\theta(p_i)\big) \Big) \Bigg) \tag{25b}$$

$$\frac{\mathrm{dSOC}_i}{\mathrm{d}p_i} = \frac{-P_{b,i}\left(v_i, F_{M,i}\right)}{E_{b,\max,i}}, \tag{25c}$$

resulting in the state vector $x_i(p_i) = [t_i(p_i), v_i(p_i), \text{SOC}_i(p_i)]$ and the input vector $u_i(p_i) = [F_{M,i}(p_i), M_{\text{CVT},i}(p_i)]$.

IV. Optimal control problem and decomposition strategy

This section states the optimal control problem and proposes a decomposition strategy that obtains a solution with the benefit of reducing the computation complexity. The optimal control problem is assembled using the defined vehicle model and constraints and aims at achieving close-to-optimal energy efficiency and vehicle throughput. The decomposition strategy "splits" the optimization problem into two stages: first the heuristic retrieval of a crossing order related to all MUTEX constraints and second the computation of optimal trajectories under these crossing orders.

A. Optimal Coordination Problem

The problem of finding energy-efficient vehicle trajectories that avoid collisions can be stated as:

***Problem** 2:* (Energy-efficient coordination problem) Obtain the optimal state and control trajectories $\mathcal{X}^* = \{x_1^*, ..., x_{N_a}^*\}$, $\mathcal{U}^* = \{u_1^*, ..., u_{N_a}^*\}$, given the initial state $\mathcal{X}_0 = \{x_{1,0}, ..., x_{N_a,0}\}$, by solving the optimization problem

$$\min_{\mathcal{X},\mathcal{U},\mathcal{O}^{\mathcal{I}},\mathcal{O}^{\mathcal{MS}},\mathcal{O}^{\mathcal{CS}}} \sum_{i=1}^{N_a} \int_{p_{i,0}}^{p_{i,M_i}} \left(Q_i P_{b,i} + H_i a_i(p_i)^2 \right) \frac{\mathrm{d}p_i}{v_i(p_i)} + R_i t_i(p_{i,M_i}) \tag{26a}$$

$$\text{s.t} \quad \text{initial states} \;\; x_{i,0} = \hat{x}_{i,0}, \forall i \tag{26b}$$

$$\text{system dynamics (25)}, \;\; \forall i \tag{26c}$$

$$\text{state and input constraints (15)} - \text{(17)}, \text{(19)}, \text{(22)} - \text{(24)}, \;\; \forall i \tag{26d}$$

$$\text{safety constraints (7),(8), (10)}, \;\; \forall i \tag{26e}$$

where p_{i,M_i} indicates the end position for vehicle i, Q_i, H_i and $R_i \in \mathbb{R}$ are the cost function weight parameters. For each vehicle, the cost function consists of minimizing the squares of the acceleration, the power of the battery, and the end time. The first term is related to energy-efficient driving while the second term is related to driving comfort and component wear. Furthermore, acceleration is a function of the propulsion force that indirectly influences power consumption. Therefore, minimizing the acceleration is desirable for the use case investigated in this paper. The last term "motivates" the vehicles to arrive at their end destination as fast as possible, i.e., it affects to mission end time.

B. Decomposition Strategy

The coordination problem, Problem 2, can be stated as a Mixed Integer Nonlinear Program (MINLP), where the crossing order corresponds to the "integer part" and the state and control trajectories correspond to the "NLP part". In essence, we can state Problem 2 in the general form as

$$\min_{\mathcal{W},b} \;\; J(\mathcal{W}) \tag{27a}$$

$$\text{s.t.} \;\; g(\mathcal{W}) = 0 \tag{27b}$$

$$h(\mathcal{W}) \leq 0 \tag{27c}$$

$$c(\mathcal{W}, b) \leq 0, \tag{27d}$$

where $\mathcal{W} = \{\mathcal{X}, \mathcal{U}\}$, $J(\mathcal{W}) = \sum_{i=1}^{N_a} J_i\left(w_i\right)$, $g(\mathcal{W}), h(\mathcal{W})$ gather all equality and inequality constraints, and $c(\mathcal{W}, b) = c_w(\mathcal{W}) + Cb$ are the integer constraints for the combinatorial part of the problem with C being a matrix that captures the influence of the integer variables.

As explained in [31], [32], finding a solution to MINLP problems is known to be difficult, especially when the constraints or the objective function are non-convex [37]. Therefore, a common procedure is to apply an approach where the integer part of the solution is obtained first using a heuristic, and the continuous part of the solution thereafter is obtained by solving the nonlinear program (NLP) that results from fixing the integers to the values found with the heuristic. The heuristic that is used is similar to that of [32] which approximates the integer part of the solution of (26) by solving a Mixed Integer Quadratic Problem (MIQP). With the obtained integer solution, the state and control trajectories are calculated by solving the "fixed-order coordination" NLP, i.e., Problem 2 with fixed crossing orders $\mathcal{O}^{\mathcal{I}}$, $\mathcal{O}^{\mathcal{MS}}$, $\mathcal{O}^{\mathcal{CS}}$.

1) Crossing Order Heuristic: The MIQP that is assembled for obtaining the crossing order is formed as a quadratic approximation of (27). The way we form the quadratic approximation is similar to how the QP sub-problems are formed in Sequential Quadratic Programming (SQP) methods [38]. In essence, we can reformulate (27) as:

$$\min_{\Delta\mathcal{W},b} \ \frac{1}{2}\begin{bmatrix}\Delta\mathcal{W}\\ b\end{bmatrix}^T \mathbf{H}(\mathcal{W},\lambda,\mu)\begin{bmatrix}\Delta\mathcal{W}\\ b\end{bmatrix} + \nabla_{\mathcal{W}} J(\mathcal{W})^T\begin{bmatrix}\Delta\mathcal{W}\\ b\end{bmatrix} + J(\mathcal{W}^{**}) \tag{28a}$$

$$\text{s.t.} \quad g(\mathcal{W}^{**}) + \nabla_{\mathcal{W}} g(\mathcal{W}^{**})^T\begin{bmatrix}\Delta\mathcal{W}\\ b\end{bmatrix} = 0 \tag{28b}$$

$$h(\mathcal{W}^{**}) + \nabla_{\mathcal{W}} h(\mathcal{W}^{**})^T\begin{bmatrix}\Delta\mathcal{W}\\ b\end{bmatrix} \le 0 \tag{28c}$$

$$c_w(\mathcal{W}^{**}) + \nabla_{\mathcal{W}} c_w(\mathcal{W}^{**})^T\begin{bmatrix}\Delta\mathcal{W}\\ b\end{bmatrix} + Cb \le 0, \tag{28d}$$

where $\mathbf{H}(\mathcal{W},\lambda,\mu) = \text{blkdiag}\left(\{H_i\}_{i=1}^{N_a}, \mathbf{0}_{n_0,n_0}\right)$ is a block diagonal matrix with positive definite $H_i(w_i,\lambda_i,\mu_i) = \nabla^2_{w_i}\mathcal{L}(w_i,\lambda_i,\mu_i) = \nabla^2_{w_i} J_i(w_i) - \nabla^2_{w_i}\lambda_i^T g(w_i) - \nabla^2_{w_i}\mu_i^T h(w_i)$, where λ_i, μ_i are the dual variables and $\mathbf{0}_{n_0,n_0}$ zeros of appropriate size for the integer variables, $n_0 = r_0 + w_0 + e_0$ being the total amount of MUTEX zones, and $\Delta\mathcal{W} = \mathcal{W} - \mathcal{W}^{**}$, with a solution guess $\mathcal{W}^{**}$. The MIQP problem (28) can be compactly written as

$$\min_{\mathcal{W},b} \ \frac{1}{2}\begin{bmatrix}\mathcal{W}\\ b\end{bmatrix}^T \mathbf{H}\begin{bmatrix}\mathcal{W}\\ b\end{bmatrix} + \mathbf{J}^T\begin{bmatrix}\mathcal{W}\\ b\end{bmatrix} + \alpha \tag{29a}$$

$$\text{s.t.} \quad A_{\text{eq}}\begin{bmatrix}\mathcal{W}\\ b\end{bmatrix} = b_{\text{eq}} \tag{29b}$$

$$A_{\text{ineq}}\begin{bmatrix}\mathcal{W}\\ b\end{bmatrix} \le b_{\text{ineq}}, \tag{29c}$$

where $\mathbf{J}$ now contains all the first order terms, α contains the linear terms and where the constraints (28b)-(28d) are grouped into equality constraints $A_{\text{eq}}, b_{\text{eq}}$ and inequality constraints $A_{\text{ineq}}, b_{\text{ineq}}$, respectively. The solution to the MIQP problem provides crossing orders $\hat{\mathcal{O}}^{\mathcal{I}}$, $\hat{\mathcal{O}}^{\mathcal{MS}}$, $\hat{\mathcal{O}}^{\mathcal{CS}}$ that is obtained from the values of the integer variables b and are optimal for the approximated problem.

Remark 6: The crossing orders obtained from the MIQP are optimal solutions for the given problem. However, as the MIQP is an approximation of the MINLP, the crossing orders resulting from the MIQP could be sub-optimal for the MINLP.

Remark 7: We make the simplification that the dual variables (λ_i, μ_i) are equal to zero. This results in that H_i only includes the second order expansion of the cost function, i.e., $H_i(w_i) = \nabla^2_{w_i} J_i(w_i)$.

Remark 8: In practice, there is no restriction on the solution guess $\mathcal{W}^{**}$ as long as it is a feasible solution. A solid solution guess can be obtained, for example, by solving the optimization problem (26) without safety constraints (26e), or through a forward simulation of the vehicles with, for example, a simple feedback controller. It is also important to note that the heuristic is more sensitive to poor solution guesses if the vehicles have limited control authority, for example, if the vehicles are in a close proximity to a MUTEX zone.

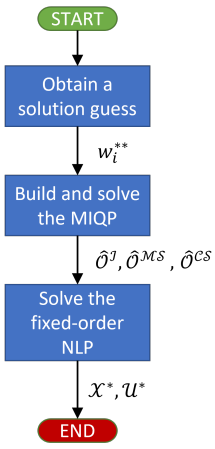

Fig. 4. Flow chart illustrating the two-stage approach.

2) Fixed-order NLP: With the found crossing order, problem (26) is reduced to an NLP as all other integer solutions are removed. Obtaining the optimal state and control trajectories is thus found through solving the *fixed-order coordination problem*

$$\min_{x_i,u_i} \ \sum_{i=1}^{N_a}\int_{p_{i,0}}^{p_{i,M_i}} \left(Q_i P_{b,i} + H_i a_i(p_i)^2\right)\frac{\mathrm{d}p_i}{v_i(p_i)} + R_i t_i(p_{i,M_i}) \tag{30a}$$

$$\text{s.t} \quad \text{(26b)} - \text{(26e)}, \ \forall i \tag{30b}$$

$$\mathcal{O}^{\mathcal{I}} = \hat{\mathcal{O}}^{\mathcal{I}}, \ \ \mathcal{O}^{\mathcal{MS}} = \hat{\mathcal{O}}^{\mathcal{MS}}, \ \ \mathcal{O}^{\mathcal{CS}} = \hat{\mathcal{O}}^{\mathcal{CS}} \tag{30c}$$

The two-stage approximation approach described in this section that solves Problem 2 is summarized in Algorithm 1 and illustrated in Figure 4.

Algorithm 1 Two-stage approximation algorithm

Input: $N_a, \mathcal{I}, \mathcal{Q}_r, \mathcal{MS}, \mathcal{Z}_w, \mathcal{CS}, \mathcal{G}_v$, vehicle paths
Output: $\mathcal{X}^*$, $\mathcal{U}^*$

1: $\forall i$: Obtain a solution guess w_i^{**} by, e.g., solving NLP (26) w/o the safety constraints (26e).
2: Calculate and form the terms $\mathbf{H}, \mathbf{J}, \alpha$.
3: Solve the MIQP (29) to get crossing orders $\hat{\mathcal{O}}^{\mathcal{I}}$, $\hat{\mathcal{O}}^{\mathcal{MS}}$, $\hat{\mathcal{O}}^{\mathcal{CS}}$.
4: Solve the fixed-order NLP (30) using $\hat{\mathcal{O}}^{\mathcal{I}}$, $\hat{\mathcal{O}}^{\mathcal{MS}}$, $\hat{\mathcal{O}}^{\mathcal{CS}}$ to obtain $\mathcal{X}^*$, $\mathcal{U}^*$.

V. Simulations

In this section, we present the simulation scenario as well as the baselines and performance metrics that are used for the comparative analysis of the vehicles' behavior.

A. Simulation Setup

We consider a mock-up confined site with a layout shown in Figure 5. The confined site consists of 5 vehicles with one charging station, one narrow road, and multiple merge-split zones and path intersections, summarized in Table I. Since Vehicle 1 and 4, and Vehicle 2 and 3 have the same starting

TABLE I
MUTEX ZONES FOR THE SCENARIO ILLUSTRATED IN FIGURE 5

	Zone set	Vehicle set
Intersections and narrow roads	$\mathcal{I} = \{I_1, I_2, I_3\}$	$\mathcal{Q}_1 = \{1, 4, 5\}$ $\mathcal{Q}_2 = \{2, 5\}$ $\mathcal{Q}_3 = \{3, 5\}$
Merge-splits	$\mathcal{MS} = \{MS_1, MS_2, MS_3, MS_4, MS_5\}$	$\mathcal{Z}_1 = \{1, 4\}$ $\mathcal{Z}_2 = \{2, 3\}$ $\mathcal{Z}_3 = \{1, 2, 3, 4\}$ $\mathcal{Z}_4 = \{3, 4\}$ $\mathcal{Z}_5 = \{1, 2, 3, 4\}$
Charging stations	$\mathcal{CS} = \{CS_1\}$	$\mathcal{G}_1 = \{1, 2\}$

point, we need to enforce rear-end collision constraints from the start. Every vehicle starts from an initial velocity of 50 [km/h] and Vehicle 3, 4, and 5 start from a nonzero initial time to ensure that a collision occurs if no coordinating action is taken. The initial times for the three vehicles are $t_{3,0} = 0.5$, $t_{4,0} = 4$, $t_{5,0} = 54$ seconds. Table V in the Appendix gathers the rest of the numerical values of the parameters that are used in the simulations.

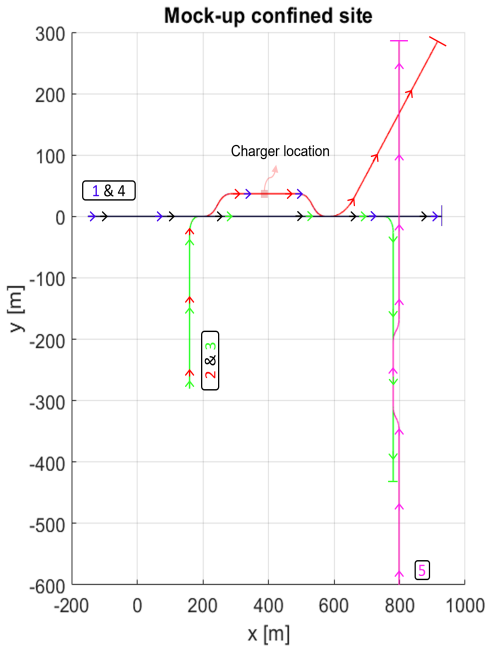

Fig. 5. Mock-up confined site area consisting of five vehicles indicated with different colors, one charging station and narrow road, and multiple merge-splits and intersections.

The modeling and simulation aspects are implemented in MATLAB. We utilize the CasADi toolkit, [39], and IPOPT, [40], to formulate and solve the NLP optimization problem (30) and use Gurobi for the MIQP (29).

Remark 9: The independent variable p_i is discretized as $p_i = (p_{i,0}, \ldots, p_{i,M_i})$, where the input is approximated using zero-order hold such that $u(p) = u_{i,k}, p \in [p_{i,k}, p_{i,k+1}[$. The equations are (numerically) integrated on this grid.

B. Baselines

We compare the proposed MIQP-based heuristic with two baselines relying on different strategies for obtaining the crossing order: a "predictive" first-come-first-serve (FCFS) approach and a rule-based one.

1) Predictive First-Come-First-Serve Heuristic: The crossing order is determined based on a first-come-first-serve approach, and then the fixed-order NLP (30) is solved utilizing the long horizon to make the necessary changes in the state and control trajectories such that the order is obeyed. The "predictive" part is that the crossing order is obtained for all MUTEX zones the vehicle encounters instead of obtaining the crossing order when the vehicles are close to the zone. To obtain the crossing order, for each vehicle, we need to compute the entry times for all MUTEX zones the vehicle encounters. Then for every MUTEX zone, the crossing order is assigned based on the lowest entry times. The heuristic is summarized in Algorithm 2.

Algorithm 2 First-come-first-serve heuristic

Input: $N_a, \mathcal{I}, \mathcal{Q}_r, \mathcal{MS}, \mathcal{Z}_w, \mathcal{CS}, \mathcal{G}_v$, vehicle paths
Output: $\mathcal{X}^*$, $\mathcal{U}^*$

1: $\forall i$: Obtain entry times for all MUTEX zones the vehicle encounters by, e.g., solving NLP (26) w/o the safety constraints (26e).
2: Using the First-Come-First-Serve logic, fix the crossing orders $\hat{\mathcal{O}}^{\mathcal{I}}$, $\hat{\mathcal{O}}^{\mathcal{MS}}$, $\hat{\mathcal{O}}^{\mathcal{CS}}$.
3: Solve the fixed-order NLP (30) using $\hat{\mathcal{O}}^{\mathcal{I}}$, $\hat{\mathcal{O}}^{\mathcal{MS}}$, $\hat{\mathcal{O}}^{\mathcal{CS}}$ to obtain $\mathcal{X}^*$, $\mathcal{U}^*$.

As can be noticed, the first and last steps of the heuristic are identical to the heuristic in Algorithm 1. The benefit of this heuristic is that the computational effort for computing the crossing orders is almost negligible in comparison to the MIQP-based heuristic, however, the crossing order could be sub-optimal.

2) Rule-Based Heuristic: Rule-based strategies are commonly implemented in practice since the approach can be formulated without the need for optimization. Although "simple" to implement, these approaches struggle with issues such as optimality, scalability, and feasibility. Essentially, to improve the performance the rules will have to be modified for every different use case (i.e., every different confined site).

In this paper, the rule-based approach is formed such that all vehicles are stepped through time and the rules for the MUTEX zone occupancy are developed to give access to the zone to the first vehicle that enters an area around the zone. The area around the zone is created with an additional 20-meter margin from the entry point to the zone such that vehicles arriving later can stop if necessary. We deploy a Model Predictive Control (MPC) scheme for each vehicle to control the vehicle behavior over time [41]. The MPC is structured such that the cost function is the same as the NLP problem (30) and uses the same dynamics and state and input constraints, but reformulated in the time domain. For the MUTEX zone occupancy constraints, the MPC is also subject to position constraints that are imposed at specific time steps. The MPC is created with five seconds prediction and control horizon. The MPC prediction horizon and the additional margin added to the zone is sufficient for a vehicle to make a full stop from $\overline{v}_i$.

Remark 10: Note that, as mentioned, it is possible to modify the rules such that a desired zone occupancy takes place. The zone occupancy logic could be based on intuitive knowledge to attempt to achieve the preferred vehicle behavior. One example could be to prioritize a heavier loaded vehicle that is on a road with a high slope angle instead of an unloaded vehicle that is approaching a shared MUTEX zone, even if the loaded vehicle arrives slightly later in the zone.

Remark 11: The predictive FCFS heuristic in essence is a rule-based approach combined with the benefit of long-horizon optimization through the fixed-order NLP.

C. Performance Metrics

In order to assess the performance of the algorithms, we compare the power consumption, the cumulative sum of the power consumption, the cumulative sum of the objective function, and the mission end time. The power consumption can be defined as

$$P_{\text{consum},i} = F_{M,i}(p_i)v_i(p_i). \tag{31}$$

The cumulative sum of the objective function gives a performance benchmark of how the heuristics perform with respect to the overall goals throughout the simulation scenario. The mission end time indicates when the vehicles have reached their end destination and as a performance metric is connected to the throughput of the confined site.

VI. Results and Discussion

This section summarizes the results of the comparison of the proposed heuristic with respect to the alternative approaches.

A. Scenario evaluation

The speed profiles for the complete scenario for all vehicles are depicted in Figure 6. It can be noticed that with the rule-based approach Vehicle 3 has to make a full stop for Vehicle 5 before the narrow road zone. Narrow roads present a particular difficulty for the rule-based approaches as the shared narrow road, in most cases, is long. For our implementation specifics of the rule-based approach, in the cases when the zone is longer than the prediction horizon, there is a "risk" that one of the vehicles would be required to make a full-stop and wait. The MIQP-based and predictive FCFS heuristics manage to avoid full stops with adequate long-term changes. We can also notice the moment when Vehicle 1 and Vehicle 2 stop at the charging station. Both vehicles are charged for 30 minutes (1800 seconds) and leave the charging station with a 14% increased state of charge. As Vehicle 2 enters the charging zone after Vehicle 1 it is also required to wait for Vehicle 1 to leave the charging station before it can start charging its battery. Furthermore, it is important to note that both the MIQP-based heuristic and the predictive FCFS approach result in the same motion profile for Vehicle 1 and Vehicle 2.

Figure 7 gives a comparison between the vehicle trajectories obtained with the different heuristics that are entering the merge-split zone located before the charging station. The zone is shared between four vehicles and is 40 meters long. The

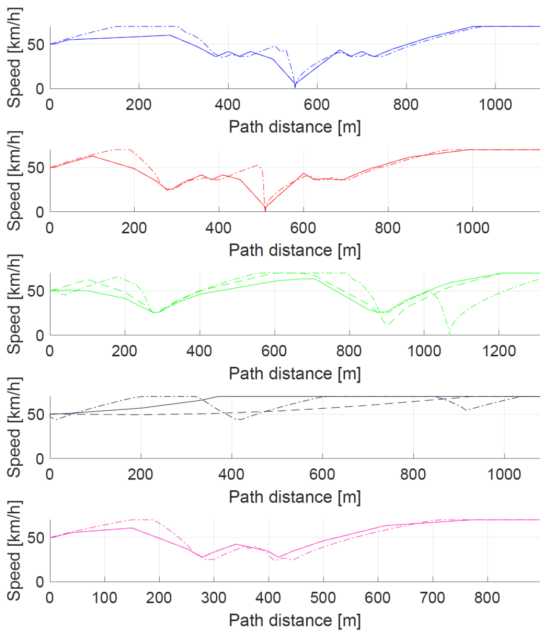

Fig. 6. Speed profiles for the vehicles in the scenario depicted in Figure 5. The solid line trajectories are obtained from the MIQP-based heuristic, the dashed lines from the predictive FCFS, and the dashed-dotted lines from the rule-based approach. The color of the lines represents the vehicles as described in Figure 5.

trajectories have an offset such that a position of zero indicates when the vehicle enters the zone. Furthermore, the time is offset by the time the first vehicle enters the zone, resulting in the highest priority vehicle entering the zone at time zero and position zero. For the displayed time vs. position dependency, the trajectories of the vehicles must not intersect while in the zone and keep the defined gap in equation (8).

As can be seen from the figure, all heuristics successfully manage to satisfy the collision constraints. The difference comes in the order in which the vehicles occupy the zone and the trajectory profile. It can be noticed that the MIQP-based heuristic has "switched" the order of Vehicle 3 and Vehicle 4, allowing Vehicle 4 to enter the zone first even though, if uncoordinated, it does not arrive at the zone before Vehicle 3. It can also be noticed from Figure 7 the difference in the trajectory profile for Vehicle 3 and Vehicle 4. Due to the full horizon perspective of the predictive FCFS, the heuristic is aware that Vehicle 3 in the later part of the road will have to slow down for the 90-degree turn and thus makes slight changes in the speed profile of Vehicle 4 from the beginning, while also "pushing" Vehicle 3 to the minimum gap to Vehicle 2. On the other hand, the rule-based approach is trying to maximize the distance the vehicles cover for their horizon, resulting in harsher speed changes at later instances.

Table II provides the crossing orders for all MUTEX zones. The merge-split zones, involving Vehicle 3 and Vehicle 4, are the specific areas where the MIQP approach produces distinct crossing orders. In these zones, the MIQP switches the occupancy order for these vehicles, which aligns with the observed behavior depicted in Figure 7.

Table III summarizes the end times for all vehicles using

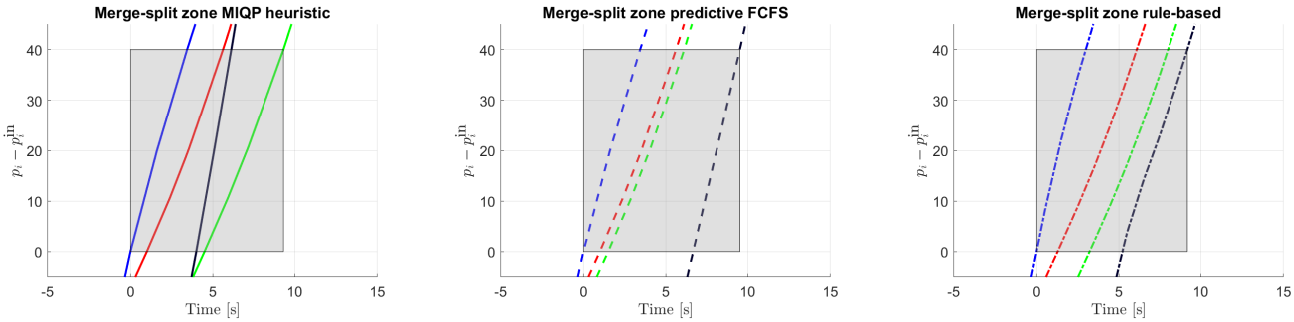

(a) Zone occupancy using the MIQP-based heuristic (b) Zone occupancy using the predictive FCFS heuristic (c) Zone occupancy using the rule-based heuristic

Fig. 7. Zone occupancy with the different heuristics. The gray zone depicts the merge-split zone that in this case is 40 meters long and the occupancy times from when the vehicle with the highest order enters the zone until the lowest order vehicle exits the zone. Any intersection between the trajectories is indicating that a collision occurs inside the zone. The color of the lines represents the vehicles as described in Figure 5.

the different approaches. From the table, we can also notice the influence of the charging time on the time the vehicles arrive at their end destination. Furthermore, if we compare the end times for the different heuristics we can conclude that the MIQP-based heuristic results in overall the lowest end times due to the "improved" MUTEX zone priority. The improved performance of the MIQP-based heuristic with respect to the other baselines is also noticeable through the power consumption and objective function performance metrics illustrated in Figure 8 and Figure 9. Figure 10 summarizes the average end time, the average power consumption, and the cumulative sum of the cost function for the approaches. The values are scaled by the values of the MIQP-based approach, i.e., the MIQP-based approach has a value of 1 in the diagram. There are minor differences in the average end time for the heuristics, in particular, the average end times for the MIQP-based approach, the predictive FCFS, and the rule-based approach are 1180.4, 1182.2, and 1184.4 seconds, respectively. If we are only focusing on the scenario end time, then the rule-based approach achieves the best scenario end time as Vehicle 2 for this approach ends its mission before the other approaches. However, Vehicle 3, Vehicle 4 and Vehicle 5 for the MIQP approach end their mission earlier than the rule-based approach, thus allowing them to continue with other tasks earlier than they would for the rule-based approach. In terms of energy consumption, for the analyzed scenario, the proposed heuristic achieves a 5.4 % and a 7.6 % improvement compared to the predictive FCFS and the rule-based approaches, respectively. It is worth noting that this is just one run of a mock-up mission given by a mock-up path planner. Any improvements on one run are even more significant taking that the vehicles operate on the site for long periods of time and will result in a considerable overall performance benefit.

Remark 12: The predictive FCFS heuristic is overall a fairly good approach that comes at a "cheaper" computational price than the MIQP-based heuristic. Depending on the scenarios and initial conditions the predictive FCFS can give a solution of the same quality as the MIQP-based heuristic. In fact, if the start time for Vehicle 4 is $t_{4,0} = 0.5$ seconds for the scenario in Figure 5, the predictive FCFS and the MIQP-based heuristic will provide the same solution in terms of crossing order and state and input trajectories. However, there are scenarios when the predictive FCFS heuristic will constantly give suboptimal solutions as further discussed in VI-C. It is also worth noting that throughout other simulation scenarios that were performed, but not included in this paper, the predictive FCFS never gave a better solution than the MIQP-based approach.

TABLE II
SETS OF CROSSING ORDER FOR ALL MUTEX ZONES IN THE CONFINED SITE.

	MIQP	FCFS	Rule-based
I_1	$\mathcal{O}_1^{\mathcal{I}} = \{4,5,1\}$	$\mathcal{O}_1^{\mathcal{I}} = \{4,5,1\}$	$\mathcal{O}_1^{\mathcal{I}} = \{4,5,1\}$
I_2	$\mathcal{O}_2^{\mathcal{I}} = \{5,2\}$	$\mathcal{O}_2^{\mathcal{I}} = \{5,2\}$	$\mathcal{O}_2^{\mathcal{I}} = \{5,2\}$
I_3	$\mathcal{O}_3^{\mathcal{I}} = \{5,3\}$	$\mathcal{O}_3^{\mathcal{I}} = \{5,3\}$	$\mathcal{O}_3^{\mathcal{I}} = \{5,3\}$
MS_1	$\mathcal{O}_1^{\mathcal{MS}} = \{1,4\}$	$\mathcal{O}_1^{\mathcal{MS}} = \{1,4\}$	$\mathcal{O}_1^{\mathcal{MS}} = \{1,4\}$
MS_2	$\mathcal{O}_2^{\mathcal{MS}} = \{2,3\}$	$\mathcal{O}_2^{\mathcal{MS}} = \{2,3\}$	$\mathcal{O}_2^{\mathcal{MS}} = \{2,3\}$
MS_3	$\mathcal{O}_3^{\mathcal{MS}} = \{1,2,4,3\}$	$\mathcal{O}_3^{\mathcal{MS}} = \{1,2,3,4\}$	$\mathcal{O}_3^{\mathcal{MS}} = \{1,2,3,4\}$
MS_4	$\mathcal{O}_4^{\mathcal{MS}} = \{4,3\}$	$\mathcal{O}_4^{\mathcal{MS}} = \{3,4\}$	$\mathcal{O}_4^{\mathcal{MS}} = \{3,4\}$
MS_5	$\mathcal{O}_5^{\mathcal{MS}} = \{4,3,1,2\}$	$\mathcal{O}_5^{\mathcal{MS}} = \{3,4,1,2\}$	$\mathcal{O}_5^{\mathcal{MS}} = \{3,4,1,2\}$
CS_1	$\mathcal{O}_1^{\mathcal{MS}} = \{1,2\}$	$\mathcal{O}_1^{\mathcal{MS}} = \{1,2\}$	$\mathcal{O}_1^{\mathcal{MS}} = \{1,2\}$

TABLE III
COMPARISON OF THE VEHICLE'S END TIME WITH THE DIFFERENT HEURISTICS IN SECONDS

	Vehicle 1	Vehicle 2	Vehicle 3	Vehicle 4	Vehicle 5
MIQP	1906	3712	101	64	119
FCFS	1906	3712	102	73	119
RB	1902	3709	117	71	122

B. Computational demand

The approaches have different computational complexities. The simulation scenario is implemented in MATLAB on a 2.10GHz 12th Gen Intel i7 with 32GB of RAM. The MIQP-based heuristic and the predictive FCFS algorithms share their first and last step. For both approaches solving the NLP (26) without the safety constraints (26e) requires 0.406 seconds in total. For obtaining the crossing order the MIQP-based approach requires 0.04 seconds to solve the MIQP (29), while for the predictive FCFS, the computation time is negligibly small (0.00148 seconds). This computational improvement is

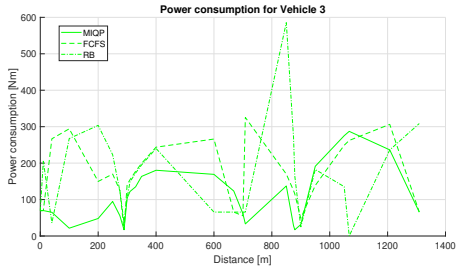

(a) Power consumption over distance for Vehicle 3

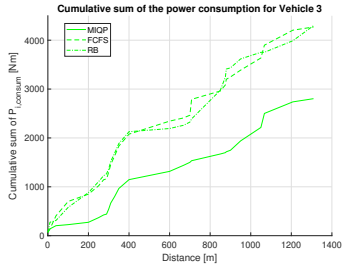

(b) Cumulative sum of the power consumption for Vehicle 3

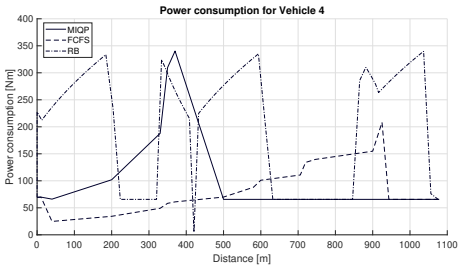

(c) Power consumption over distance for Vehicle 4

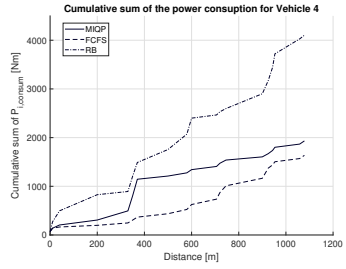

(d) Cumulative sum of the power consumption for Vehicle 4

Fig. 8. Comparison of the power consumption and the cumulative sum of the power consumption for vehicles 3 and 4. The full line trajectories are obtained from the MIQP-based heuristic, the dashed lines from the predictive FCFS, and the dashed-dotted lines from the rule-based approach. The color of the plots represents the vehicles as described in Figure 5.

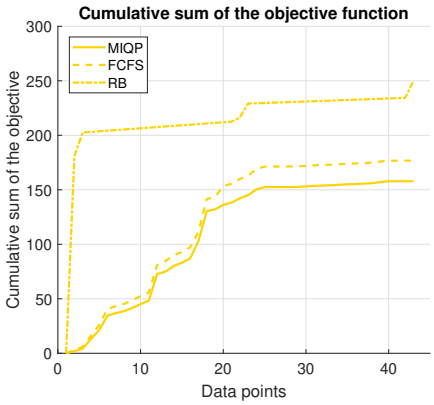

Fig. 9. Cumulative sum of the objective function for the investigated heuristics. The full line trajectories are obtained from the MIQP-based heuristic, the dashed lines from the predictive FCFS, and the dashed-dotted lines from the rule-based approach.

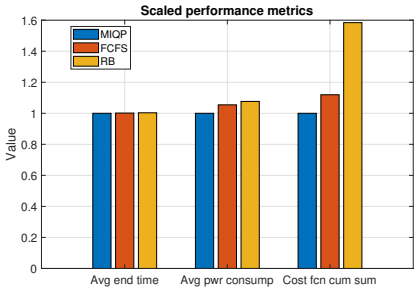

Fig. 10. Summary of the performance metrics for the presented approaches. The values of the performance metrics are scaled by values of the MIQP-based heuristic.

the main benefit of the FCFS heuristic with respect to the MIQP-based heuristic. Finally, solving the fixed order NLP (30) with the found crossing order requires 0.664 seconds for the MIQP-based heuristic and 1.41 seconds for the predictive FCFS. The reason for the increased computational demand of the predictive FCFS fixed order NLP is the different MUTEX occupancy order. As we can notice a different crossing order can result in a significant difference that could neglect the computational improvement for obtaining the crossing order. The rule-based logic takes an insignificant amount of time (0.0003) seconds. The "light" computational effort is often the main appeal of using a rule-based approach.

Remark 13: The computational complexity of the MIQP-based heuristic is exponential in the number of decision variables, i.e., the number of MUTEX zones, while the computational complexity of the fixed-order NLP is cubic with the number of vehicles, which includes the sum of N_a vehicles and M_i discretization points per vehicle. This means that the heuristic could be impractical for large problem formulations. However, the confined sites that are currently found in practice, do not pose this restriction.

C. Predictive FCFS "suboptimality"

In the previous example, we could notice that the predictive FCFS heuristic underperforms with respect to the MIQP-based heuristic. This result is due to that the crossing order is solely determined by who enters the MUTEX zone first. The suboptimal behavior of the predictive FCFS heuristic is particularly amplified in long narrow road zones as depicted in Figure 11. The suboptimality in these scenarios occurs when the vehicle coming from the loop part of the road (depicted

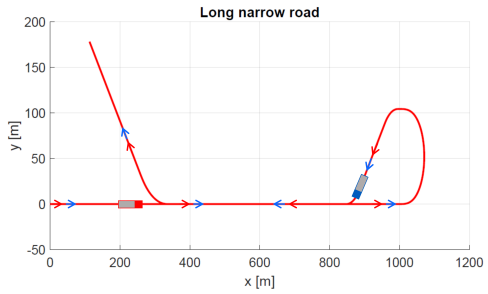

Fig. 11. Long narrow road scenario.

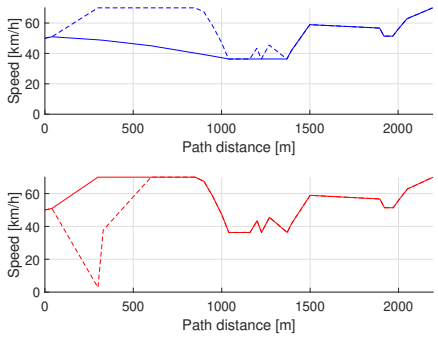

Fig. 12. Speed profiles for the MIQP-based and the predictive FCFS heuristics for the long narrow road scenario.

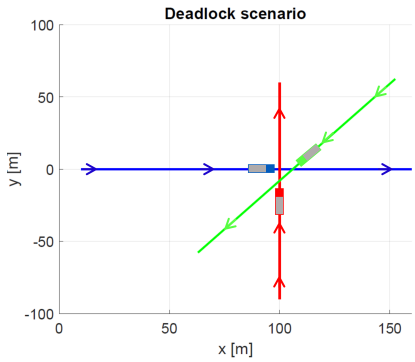

Fig. 13. Scenario where a deadlock can occur.

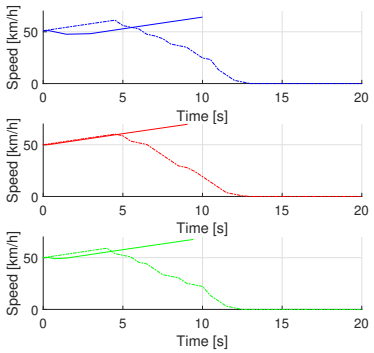

Fig. 14. Speed profiles with respect to the simulation time. The solid lines represent the MIQP-based approach.

as the blue vehicle) enters the zone before the vehicle coming from the straight part of the road (the red vehicle). The MIQP-based heuristic uses the knowledge that the blue vehicle has to slow down for the turns in the loop to switch the order such that the red vehicle that is on the straight part of the road will not have to make "harsh" changes to its speed profile, thus improving overall energy efficiency. Figure 12 depicts the speed profiles when the vehicles are initialized such that this suboptimality occurs. The start time for Vehicle 2 (red vehicle) is 72 seconds which results in the vehicle entering the zone just after the blue vehicle. The total objective function value for the MIQP-based heuristic for this scenario is 3.83 kJ and for the predictive FCFS is 3.95 kJ. The cumulative sum of the power consumption for Vehicle 1 and 2 using the MIQP-based heuristic is 2.35 kJ and 3.88 kJ, respectively, while for the predictive FCFS these values are 3.88 kJ and 3.98 kJ, resulting in a significant increase.

D. Deadlocks

In addition to the subpar performance, another drawback of the rule-based approach is that it is not able to avoid deadlocks in all cases. A deadlock occurs when two or more vehicles are not able to move as they are blocked by another vehicle and consequently are blocking a part of the road that should be used by another vehicle. This behavior can occur in rule-based approaches as the method is not considering more than one zone at a time, [42]. On the other hand, the MIQP-based heuristic is capable of avoiding deadlocks as the obtained order considers the evolution of the state and input trajectories over the whole horizon that covers all occurring MUTEX zones. This means that the order will be adjusted such that the vehicles reach their end destination.

An illustrative example of deadlocks and deadlock avoidance is shown in Figure 13, Figure 14, and Figure 15, where Figure 13 depicts the scenario and Figure 14, and Figure 15 depict the motion of the vehicles with respect to time and distance, respectively. From Figure 13 we can notice the potential for a deadlock, i.e., a deadlock can occur because a vehicle is forced to be stopped inside a MUTEX zone and cannot continue further because another vehicle occupies the next zone, thus being blocked and blocking another vehicle. As can be seen in Figure 14, and Figure 15, the described deadlock scenario will occur if the rule-based approach is used. All vehicles are stopped (zero velocity) and the simulation has to be manually terminated. On the other hand, the MIQP-based heuristic avoids the deadlock by finding a crossing order such that the vehicles arrive at their end destination, and furthermore by utilizing the long horizon it makes adequate changes in the motion profile without the necessity for any "harsh" control actions.

Remark 14: Note that deadlocks using the rule-based approach can occur in scenarios as shown in Figure 11. This is due to that the loop section has a limited vehicle queue capacity. The deadlock will occur if the queue capacity is full and a vehicle coming from the straight part of the road is assigned the highest priority to the zone. Then, as the queue is full, that vehicle will no longer be able to exit the zone and the vehicles will remain at zero velocity.

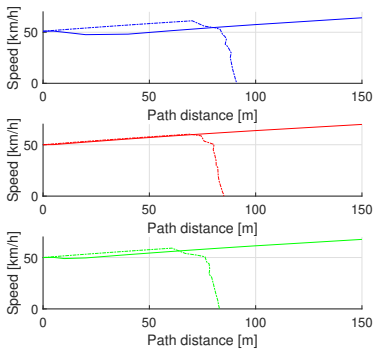

Fig. 15. Speed profiles with respect to the path distance. The solid lines represent the MIQP-based approach.

Remark 15: It is possible that in an extreme case, a solution to a deadlock problem exists but the MIQP approximation fails to capture it. In these cases, the MIQP-based heuristic will return a failure before the deadlock happens. This as we observed, is not the case when the rule-based approach is used. Additionally, in another extreme case, the MIQP may obtain a crossing order that is deemed feasible, however, the crossing order might be infeasible in the NLP. As the optimization is performed over long horizons there is sufficient time and space for a backup strategy (e.g., braking to a full stop) for the vehicles to avoid a deadlock situation or potential conflicts.

VII. Conclusions

In this paper, we have proposed and analyzed an optimization-based heuristic for high-level coordinated motion planning of an entire vehicle fleet in confined sites. By formulating the model, constraints, and objective in the spatial domain, the motion plan for the vehicles is calculated from the start until the end of their missions. The controller does not depend on a specific motion model, constraints, or a specific objective function. This flexibility allows for different vehicle model complexities and selecting an objective that specifies the desired behavior.

We have focused in this paper on electric vehicles with an energy-efficient objective function. Using this model, its constraints, and its objective we have investigated coordinating the motion of the vehicles such that conflicts are avoided in intersections, narrow roads, merge-split roads, and charging stations, where the charging of the vehicles is directly incorporated into the motion plan. The collision avoidance constraints related to these zones introduce a combinatorial dimension to the problem. The MIQP-based heuristic "splits" the problem with the first component of the heuristic computing the crossing order (i.e., solving the combinatorial part of the problem) and the second component solving for the state and input trajectories of the vehicles respecting the found crossing order. The heuristic is evaluated through simulation scenarios and compared with two alternative optimization-based heuristics. Using the simulation results we demonstrated that the MIQP-based heuristic will obtain a better or equally good crossing order and overall solution, and furthermore, the heuristic is capable of avoiding deadlock situations. Although coming with increased computational demand, it is not expected that the heuristic will be impractical for the current application focus.

The framework presented could be adapted to include additional MUTEX zones that the confined sites are comprised of, for example, loading and unloading zones. A natural extension of the work is to include the low-level controller which follows the high-level motion plan as well as developing a strategy when the high-level motion plan needs to be recomputed. Other future research directions of interest include considering mixed traffic scenarios with automated and non-automated agents, further simulation analysis with an increased number of vehicles and randomized scenario generation, and integrating an additional safety layer that can provide guarantees on the satisfaction of the collision constraints.

Appendix

The appendix consists of Table IV and V where the variables in this article and the simulation parameters are grouped.

References

[1] Bagloee, Saeed Asadi, Madjid Tavana, Mohsen Asadi, and Tracey Oliver. "Autonomous vehicles: challenges, opportunities, and future implications for transportation policies." Journal of modern transportation 24, no. 4 (2016): 284-303.

[2] Pasternak, Michal, and Joshua A. Marshall. "On the design and selection of vehicle coordination policies for underground mine production ramps." International Journal of Mining Science and Technology 26, no. 4 (2016): 623-627.

[3] Rios-Torres, Jackeline, and Andreas A. Malikopoulos. "A survey on the coordination of connected and automated vehicles at intersections and merging at highway on-ramps." IEEE Transactions on Intelligent Transportation Systems 18, no. 5 (2016): 1066-1077.

[4] Colombo, Alessandro, and Domitilla Del Vecchio. "Efficient algorithms for collision avoidance at intersections." In Proceedings of the 15th ACM international conference on Hybrid Systems: Computation and Control, pp. 145-154. 2012.

[5] Campos, Gabriel R., Paolo Falcone, Henk Wymeersch, Robert Hult, and Jonas Sjöberg. "Cooperative receding horizon conflict resolution at traffic intersections." In 53rd IEEE Conference on Decision and Control, pp. 2932-2937. IEEE, 2014.

[6] Zhang, Yue, Andreas A. Malikopoulos, and Christos G. Cassandras. "Decentralized optimal control for connected automated vehicles at intersections including left and right turns." In 2017 IEEE 56th Annual Conference on Decision and Control (CDC), pp. 4428-4433. IEEE, 2017.

[7] Hult, Robert, Mario Zanon, Sebastien Gras, and Paolo Falcone. "An miqp-based heuristic for optimal coordination of vehicles at intersections." In 2018 IEEE Conference on Decision and Control (CDC), pp. 2783-2790. IEEE, 2018.

[8] Zhang, Yue J., Andreas A. Malikopoulos, and Christos G. Cassandras. "Optimal control and coordination of connected and automated vehicles at urban traffic intersections." In 2016 American Control Conference (ACC), pp. 6227-6232. IEEE, 2016.

[9] Bang, Heeseung, Behdad Chalaki, and Andreas A. Malikopoulos. "Combined Optimal Routing and Coordination of Connected and Automated Vehicles." IEEE Control Systems Letters 6 (2022): 2749-2754.

[10] Kneissl, Maximilian, Adam Molin, Hasan Esen, and Sandra Hirche. "A feasible MPC-based negotiation algorithm for automated intersection crossing." In 2018 european control conference (ecc), pp. 1282-1288. IEEE, 2018.

[11] Riegger, Lea, Markus Carlander, Niklas Lidander, Nikolce Murgovski, and Jonas Sjöberg. "Centralized MPC for autonomous intersection crossing." In 2016 IEEE 19th international conference on intelligent transportation systems (ITSC), pp. 1372-1377. IEEE, 2016.

[12] Katriniok, Alexander, Peter Kleibaum, and Martina Joševski. "Distributed model predictive control for intersection automation using a parallelized optimization approach." IFAC-PapersOnLine 50, no. 1 (2017): 5940-5946.

TABLE IV
SUMMARY OF THE MAIN NOTATIONS USED IN THE ARTICLE. THE SUBSCRIPT i REFERS TO THE VEHICLE WITH INDEX i

Variable	Description
N_a	Number of vehicles
p_i	Vehicle position
v_i	Vehicle velocity
x_i	Vehicle state vector
u_i	Vehicle control input vector
z_i	Vector collecting remaining states
f_i	Function describing the vehicle motion
h_i	Function describing the inequality constraints
a_i	Vehicle acceleration
t_i	Vehicle travel time
p_i^{in}	Entry position to a MUTEX zone
p_i^{out}	Exit position to a MUTEX zone
t_i^{in}	Entry time to a MUTEX zone
t_i^{out}	Exit time to a MUTEX zone
$\mathcal{I}$	Set of all intersections and narrow roads
r_0	Total number of intersections and narrow roads
$\mathcal{Q}_r$	Set of vehicles crossing intersection or narrow road
$\mathcal{O}_r^{\mathcal{I}}$	Intersection or narrow road crossing order
$\mathcal{MS}$	Set of all merge-split zones
w_0	Total number of merge-split zones
$\mathcal{Z}_w$	Set of vehicles that cross the merge-split zones
$\mathcal{O}_w^{\mathcal{MS}}$	Order in which the vehicles cross a merge-split zone
Δt	Additional time gap for rear-end collision constraints
c	Additional distance gap for rear-end collision constraints
$t_{\text{charge},i}$	Charging time constant
$\underline{v}_i$	Velocity lower bound
$\mathcal{CS}$	Set of all charging station zones
e_0	Total number of charging station zones
$\mathcal{G}_v$	Set of vehicles that utilize the charging station
$\mathcal{O}_v^{\mathcal{CS}}$	Order in which the vehicles utilize the charging station
$\mathcal{X}^*$	Optimal state trajectories
$\mathcal{U}^*$	Optimal input trajectories
$\mathcal{X}_0$	Initial states
J_i	Cost function
m_i	Vehicle mass
$F_{M,i}$	Motor force
$F_{d,i}$	Aerodynamic drag force
$F_{r,i}$	Rolling resistance force
ρ	Air density
A_i	Frontal area of a vehicle
$c_{r,i}$	Rolling resistance coefficient
θ	Road gradient
$\overline{v}_i$	Velocity upper bound
$\underline{a}_{i,\text{lon}}$	Longitudinal acceleration lower bound
$\overline{a}_{i,\text{lon}}$	Longitudinal acceleration upper bound
$\overline{a}_{i,lat}$	Lateral acceleration upper bound
$\kappa_i(p_{i,k})$	Road curvature
$R_{\text{int,i}}$	Battery internal resistance
$N_{\text{cells,i}}$	Number of cells in the battery
$K_{t,i}$	Electric machine torque constant
$\underline{T}_{M,i}$	Electric machine torque lower bound
$\overline{T}_{M,i}$	Electric machine torque upper bound
$r_{w,i}$	Wheel ratio
$M_{f,i}$	Transmission's final gear ratio
$P_{b,i}$	Power of the battery
$\underline{P}_{b,i}$	Lower bound of the battery power
$\overline{P}_{b,i}$	Upper bound of the battery power
SOC_i	State of charge
$E_{b,\max,i}$	Maximum energy capacity of the battery
$\underline{\text{SOC}_i}$	State of charge lower bound
$\overline{\text{SOC}_i}$	State of charge upper bound
$M_{\text{CVT},i}$	Continuous Variable Transmission gear ration
p_{i,M_i}	End position
H_i, Q_i, R_i	Cost function weight parameters
$\mathcal{W}$	Set grouping the state and input vectors
g	Function describing the equality constraints
b	Integer variables
$c(\mathcal{W}, b)$	Integer constraints function
$\mathbf{H}$	Hessian of the objective function
$\mathbf{J}$	Jacobian of the objective function
α	Linear terms of the objective function
$\mathcal{W}^{**}$	Solution guess
$P_{\text{consum},i}$	Power consumption

TABLE V
NUMERICAL VALUES OF THE PARAMETERS USED IN THE SIMULATIONS IN SECTION V

Parameter	Definition	Numerical value
ρ	Air density	1.18 kg/m^2
A_i	Frontal area	10 m^2
m_i	Vehicle mass	23000 kg
$c_{a,i}$	Aerodynamic drag coefficient	0.5
$c_{r,i}$	Rolling resistance	0.01
$R_{\text{int,i}}$	Battery internal resistance	0.004 Ω
$N_{\text{cells,i}}$	Number of cells in the battery	180
$K_{t,i}$	Electric machine torque constant	5 Nm/A
r_w	Wheel radius	0.4 m
$E_{b,i}$	Battery capacity	184 kWh (664 MJ)
$\underline{T}_{M,i}$	Torque lower bound	-350 Nm
$\overline{T}_{M,i}$	Torque upper bound	350 Nm
$\underline{\text{SOC}_i}$	State of charge lower bound	0.1
$M_{f,i}$	Final gear ratio	20
$\underline{v}_i$	Velocity lower bound	0.1 m/s
$\overline{v}_i$	Velocity upper bound	19.44 m/s
$\underline{a}_{i,\text{lon}}$	Longitudinal acceleration lower bound	-2 m/s^2
$\overline{a}_{i,\text{lon}}$	Longitudinal acceleration upper bound	2 m/s^2
$\overline{a}_{i,lat}$	Lateral acceleration upper bound	2 m/s^2
H_i	Squares of the acceleration cost weight	1
Q_i	Power of the battery cost weight	5
R_i	End time cost weight	10
$v_{i,0}$	Initial velocity	13.89 m/s
$\text{SOC}_{i,0}$	Initial state of charge	0.6
$F_{M,i,0}$	Initial motor force	5000 N
$M_{\text{CVT},i}$	Initial gear ratio	10
$t_{\text{charge},i}$	Charge time	1800 s

[13] Mirheli, Amir, Mehrdad Tajalli, Leila Hajibabai, and Ali Hajbabaie. "A consensus-based distributed trajectory control in a signal-free intersection." Transportation research part C: emerging technologies 100 (2019): 161-176.

[14] Wuthishuwong, Chairit, and Ansgar Traechtler. "Consensus-based local information coordination for the networked control of the autonomous intersection management." Complex & Intelligent Systems 3, no. 1 (2017): 17-32.

[15] Hult, Robert, Mario Zanon, Sébastien Gros, and Paolo Falcone. "Optimal coordination of automated vehicles at intersections with turns." In 2019 18th European Control Conference (ECC), pp. 225-230. IEEE, 2019.

[16] Hult, Robert, Mario Zanon, Sébastien Gros, Henk Wymeersch, and Paolo Falcone. "Optimisation-based coordination of connected, automated vehicles at intersections." Vehicle System Dynamics 58, no. 5 (2020): 726-747.

[17] Hult, Robert, Mario Zanon, Sebastien Gros, and Paolo Falcone. "Optimal coordination of automated vehicles at intersections: Theory and experiments." IEEE Transactions on Control Systems Technology 27, no. 6 (2018): 2510-2525.

[18] Yu, Chunhui, Yiheng Feng, Henry X. Liu, Wanjing Ma, and Xiaoguang Yang. "Corridor level cooperative trajectory optimization with connected and automated vehicles." Transportation Research Part C: Emerging Technologies 105 (2019): 405-421.

[19] Zhang, Yixiao, Rui Hao, Tingting Zhang, Xiaohan Chang, Zepeng Xie, and Qinyu Zhang. "A trajectory optimization-based intersection coordination framework for cooperative autonomous vehicles." IEEE Transactions on Intelligent Transportation Systems 23, no. 9 (2021): 14674-14688.

[20] Hu, Xiangwang, and Jian Sun. "Trajectory optimization of connected and autonomous vehicles at a multilane freeway merging area." Transportation Research Part C: Emerging Technologies 101 (2019): 111-125.

[21] Hamednia, Ahad, Nalin Kumar Sharma, Nikolce Murgovski, and Jonas Fredriksson. "Computationally efficient algorithm for eco-driving over long look-ahead horizons." IEEE Transactions on Intelligent Transportation Systems (2021).

[22] Hausknecht, Matthew, Tsz-Chiu Au, and Peter Stone. "Autonomous intersection management: Multi-intersection optimization." In 2011 IEEE/RSJ International Conference on Intelligent Robots and Systems, pp. 4581-4586. IEEE, 2011.

[23] Chalaki, Behdad, and Andreas A. Malikopoulos. "Time-optimal coordination for connected and automated vehicles at adjacent intersections." IEEE Transactions on Intelligent Transportation Systems (2021).

[24] Banzhaf, Holger, Dennis Nienhüser, Steffen Knoop, and J. Marius Zöllner. "The future of parking: A survey on automated valet parking with an outlook on high density parking." In 2017 IEEE Intelligent Vehicles Symposium (IV), pp. 1827-1834. IEEE, 2017.
[25] Kneissl, Maximilian, Anil Kunnappillil Madhusudhanan, Adam Molin, Hasan Esen, and Sandra Hirche. "A multi-vehicle control framework with application to automated valet parking." IEEE Transactions on Intelligent Transportation Systems 22, no. 9 (2020): 5697-5707.
[26] Shen, Xu, Xiaojing Zhang, and Francesco Borrelli. "Autonomous parking of vehicle fleet in tight environments." In 2020 American Control Conference (ACC), pp. 3035-3040. IEEE, 2020.
[27] Wahde, Mattias, Mauro Bellone, and Sina Torabi. "A method for real-time dynamic fleet mission planning for autonomous mining." Autonomous Agents and Multi-Agent Systems 33, no. 5 (2019): 564-590.
[28] Roselli, Sabino Francesco, Per-Lage Götvall, Martin Fabian, and Knut Åkesson. "A Compositional Algorithm for the Conflict-Free Electric Vehicle Routing Problem." IEEE Transactions on Automation Science and Engineering (2022).
[29] Liu, Yubang, Shouwen Ji, Zengrong Su, and Dong Guo. "Multi-objective AGV scheduling in an automatic sorting system of an unmanned (intelligent) warehouse by using two adaptive genetic algorithms and a multi-adaptive genetic algorithm." PloS one 14, no. 12 (2019): e0226161.
[30] Zhang, Haifei, Hongwei Ge, Jinlong Yang, and Yubing Tong. "Review of vehicle routing problems: Models, classification and solving algorithms." Archives of Computational Methods in Engineering 29, no. 1 (2022): 195-221.
[31] Kojchev, Stefan, Robert Hult, and Jonas Fredriksson. "Optimization based coordination of autonomous vehicles in confined areas." In 2022 IEEE 25th International Conference on Intelligent Transportation Systems (ITSC), pp. 1957-1963. IEEE, 2022.
[32] Kojchev, Stefan, Robert Hult, and Jonas Fredriksson. "Quadratic approximation based heuristic for optimization-based coordination of automated vehicles in confined areas." In 2022 IEEE 61st Conference on Decision and Control (CDC), pp. 6156-6162. IEEE, 2022.
[33] Xiao, Lingyun, and Feng Gao. "A comprehensive review of the development of adaptive cruise control systems." Vehicle system dynamics 48, no. 10 (2010): 1167-1192.
[34] Murgovski, Nikolce, Lars Johannesson, Xiaosong Hu, Bo Egardt, and Jonas Sjöberg. "Convex relaxations in the optimal control of electrified vehicles." In 2015 American Control Conference (ACC), pp. 2292-2298. IEEE, 2015.
[35] Beachley, Norman H., and Andrew A. Frank. Continuously variable transmissions: Theory and practice. No. UCRL-15037. Lawrence Livermore National Lab.(LLNL), Livermore, CA (United States), 1979.
[36] Oglieve, Callum J., Mahdi Mohammadpour, and Homer Rahnejat. "Optimisation of the vehicle transmission and the gear-shifting strategy for the minimum fuel consumption and the minimum nitrogen oxide emissions." Proceedings of the Institution of Mechanical Engineers, Part D: Journal of Automobile Engineering 231, no. 7 (2017): 883-899.
[37] Richards, Arthur, and Jonathan How. "Mixed-integer programming for control." In Proceedings of the 2005, American Control Conference, 2005., pp. 2676-2683. IEEE, 2005.
[38] Nocedal, Jorge, and Stephen Wright. Numerical optimization. Springer Science & Business Media, 2006.
[39] Andersson, Joel AE, Joris Gillis, Greg Horn, James B. Rawlings, and Moritz Diehl. "CasADi: a software framework for nonlinear optimization and optimal control." Mathematical Programming Computation 11, no. 1 (2019): 1-36.
[40] Wächter, Andreas, and Lorenz T. Biegler. "On the implementation of an interior-point filter line-search algorithm for large-scale nonlinear programming." Mathematical programming 106, no. 1 (2006): 25-57.
[41] Rawlings James Blake David Q Mayne and Moritz Diehl. 2017. Model Predictive Control: Theory Computation and Design. 2nd ed. Madison Wisconsin: Nob Hill Publishing.
[42] Cirillo, Marcello, Federico Pecora, Henrik Andreasson, Tansel Uras, and Sven Koenig. "Integrated motion planning and coordination for industrial vehicles." In Proceedings of the International Conference on Automated Planning and Scheduling, vol. 24, pp. 463-471. 2014.

Stefan Kojchev received his M.S. degree in automotive technology from the Eindhoven University of Technology in 2018. He is currently pursuing a Ph.D. degree with the Department of Electrical Engineering, Chalmers University of Technology, Sweden in collaboration with Volvo Autonomous Solutions. His main research interests include optimal control with applications to motion planning and control of cooperative automated vehicles in confined sites.

Robert Hult received the Masters degree in Systems, Control and Mechatronics in 2013, and the Ph.D. degree in 2019, both from Chalmers University of Technology, Sweden. He is currently a Software Engineer at Volvo Autonomous Solutions in Gothenburg Sweden, working with the design and implementation of planning, control, and safety assurance functions for automated trucks and construction machines. His research interests include motion planning and control for automated vehicles, vehicle dynamics modeling, cooperative model predictive control, in particular with applications to cooperative vehicles and intelligent transportation systems, and site planning for automated vehicles in confined areas.

Jonas Fredriksson received his M.Sc. in Computer Science Engineering from Luleå University of Technology, Sweden in 1997 and Ph.D. in Automatic Control from Chalmers University of Technology, Sweden in 2002. Currently, he is a Professor in Mechatronics at the Department of Electrical Engineering at Chalmers. His research activities include modeling, control, and simulation, with a special interest in automotive applications.

Maximilian Kneissl is currently working as a Software Engineer at Volvo Autonomous Solutions in Gothenburg, Sweden. He is designing and implementing solutions for motion planning of autonomous trucking applications. He was a Research Engineer in the domains of Control and V&V for automated driving at DENSO AUTOMOTIVE Deutschland GmbH in Eching, Germany, from 2020 to 2022. He received his B.Sc., M.Sc., and Ph.D. degree in Electrical and Computer Engineering from the Technical University of Munich (TUM), Germany, in 2013, 2016, and 2021, respectively.